PERGAMON

International Journal of Heat and Mass Transfer 46 (2003) 341–354

International Journal of HEAT and MASS TRANSFER

www.elsevier.com/locate/ijhmt

Transient natural convection and conjugate transients around a line heat source

Marie-Christine Duluc [a], Shihe Xin [a,b,*], Patrick Le Quéré [a]

[a] *LIMSI-CNRS, BP 133, 91403 Orsay Cedex, France*
[b] *Dépt. de Physique, Univ. Paris Sud, 91405 Orsay Cedex, France*

Received 23 July 2001; received in revised form 5 April 2002

Abstract

Transient natural convection in liquid nitrogen around a heated wire is studied experimentally and numerically. A thin bronze wire of 40 μm in diameter and 5.1 cm in length heated by Joule effect is used in experiments and time evolutions of the wire temperature are measured through its electrical resistance. Numerical simulations of such flows are performed by using velocity–pressure formulation, spectral methods and domain decomposition technique. Experimental data and numerical results are compared and show that although the wire is extremely thin its thermal inertia plays an important role during early transients.

Scaling analyses performed for the convection set-up and transients yield $t \sim q^{-1/2}$ and $\Delta T \sim q^{3/4}$, which are confirmed by numerical simulations.

For wires heated by Joule effect hybrid thermal conditions—combined Dirichlet and Neumann conditions are proposed on the wire surface and validated by numerical simulations. On the other hand flow conditions to be imposed on the outer artificial boundary are not well known and the answer to the question remains still open: two types of flow conditions are tested and yield different velocity fields.

Keywords: External natural convection; Line heat source; Conjugate transients; Outer boundary conditions; Combined Dirichlet–Neumann conditions

1. Introduction

Natural convection around heated horizontal circular cylinders in an infinite fluid medium has been studied extensively over the last decades due to numerous technological applications. A wide range of Rayleigh numbers ($10^0 < Ra < 10^9$) has been examined experimentally and numerically for a large variety of fluids. In spite of this, new findings have recently been reported in the literature and the problem is still a current topic: in order to study transition to turbulence an experimental investigation was carried out on a cylinder heated with a uniform heat flux [1] and an analytical study dedicated to the case of very low Grashof numbers was also reported [2].

Early studies on the subject were mainly experimental [3–7] and analytical [6,8] among others. Most of them were devoted to analytical form of similarity solutions and comparisons with experimental results. Experimental data available are temperature fields measured by either interferometry or thermocouples. Instabilities are also investigated by some authors [5,7]. By the end of seventies numerical computations of similarity solutions [6,8] started. They were followed later on by attempts to solve the complete Navier–Stokes and energy equations in stream function–vorticity formulation (Ψ–ω) [9–11]. In the case of an isothermal horizontal cylinder, in order to understand discrepancy observed between the different results, Saitoh et al. [11] proposed benchmark

* Corresponding author. Address: LIMSI-CNRS, BP 133, 91403 Orsay Cedex, France. Tel.: +33-1-69-85-81-31; fax: +33-1-69-85-80-88.

E-mail address: xin@limsi.fr (S. Xin).

0017-9310/03/$ - see front matter
PII: S0017-9310(02)00266-1

Nomenclature

C_p	specific heat of liquid nitrogen at constant pressure ($J\,kg^{-1}\,K^{-1}$)
$\widetilde{C}$	specific heat of bronze ($J\,kg^{-1}\,K^{-1}$)
D	wire diameter (m)
g	gravity acceleration (m/s^2)
h	average heat transfer coefficient ($W\,m^{-2}\,K^{-1}$)
L	wire length (m)
Pr	Prandtl number ($=\nu/\kappa$)
q	heat flux (W/m^2)
Q	heat power or heat loss rate (W)
r	radial distance (m)
$\mathscr{R}$	electrical resistance of the wire (Ω)
R	wire radius (m)
R'	radial position of the outer boundary (m)
Ra	Rayleigh number ($=[g\beta(T_w - T_0)D^3]/(\nu\kappa)$)
t	time (s)
T	temperature (K)
u	radial velocity component (m/s)
v	azimuthal velocity component (m/s)
p	pressure deviation from hydrostatic pressure (N/m^2)
U	voltage (V)
β	coefficient of volumetric thermal expansion (K^{-1})
$\Delta T = T - T_0$	superheat (K)
γ	temperature coefficient of bronze (K^{-1})
κ	thermal diffusivity (m^2/s)
λ	thermal conductivity of liquid nitrogen ($W\,m^{-1}\,K^{-1}$)
$\widetilde{\lambda}$	thermal conductivity of bronze ($W\,m^{-1}\,K^{-1}$)
μ	dynamic viscosity of liquid nitrogen ($kg\,m^{-1}\,s^{-1}$)
ν	kinematic viscosity of liquid nitrogen (m^2/s)
ρ	density of liquid nitrogen (kg/m^3)
$\widetilde{\rho}$	density of bronze (kg/m^3)
θ	azimuthal position in polar system

Subscripts

f	fluid
J	Joule effect
k	wave number in Fourier space
L	per unit length
s	supports
w	wire
v	volumetric (per volume)
0	related to initial or ambient condition
1	related to the 1 Ω/8 W electrical resistance

solutions for Prandtl number of 0.7 and Rayleigh numbers ranging from 10^3 to 10^5. They used a fourth-order finite difference method, a logarithmic coordinate transformation as well as a solid outer boundary condition placed at some 1000–20 000 times the cylinder diameter. Recently, a critical Rayleigh number of 2.1×10^9 corresponding to transition of the boundary layer along the cylinder surface was determined by flow visualisation and this transition to turbulence is induced by three-dimensional effects [1]. Analytical efforts are combined with numerical methods to give a full description of flow structure close to the line-sources for very low Grashof numbers [2].

Most studies mentioned above concern steady flows and very little data about transient flows are available in the literature. Only Ostroumov [3] realised in 1956 a pioneering experimental work on transient natural convection around a platinum wire (diameter of 100 μm) following a step heating by Joule effect. Visualisation of flow fields and temperature distributions around the wire has been performed using light-scattering particles and the optical grid method respectively. A time-sequence is also given numerically by Saitoh et al. [11]. Qualitative agreement between these results is very good although in one case the cylinder surface is kept at constant temperature while in another the wire is heated by a constant power. After the heating process is switched on, the hot fluid moves up, two symmetric circulations form at each side of the cylinder and rise away as time progresses. The isotherms, in form of a mushroom, also 'grow' in time.

The present work is concerned with transient natural convection around a line heat source (very thin wire) induced by a step heating. It is mainly motivated by the onset of natural convection flow and the superheat of the line heat source following a heating step. We conducted for that purpose both numerical and experimental studies.

So far most of numerical studies on natural convection around cylinders have been realised using stream function–vorticity formulation. Only one recent work deals with velocity–pressure formulation and with the issue of prescribing appropriate boundary conditions [12]: a pressure condition is suggested. More studies under velocity–pressure formulation are therefore useful and necessary, that is why in the present work numerical simulations have been performed under velocity–pressure formulation. We are also concerned with the proper boundary conditions in the far-field because physical domains around cylinders are unbounded and one has to choose an artificial boundary in the far-field and the corresponding boundary conditions. Another

reason for using velocity–pressure formulation is due to the fact that boundary conditions of stress free type in the far-field seem more plausible, but they do not appear naturally in stream function–vorticity formulation. As the far field boundary conditions did not produce satisfactory results, Saitoh et al. were led to push away the artificial boundary and used a solid boundary (external natural convection becomes then internal natural convection), which is not optimal in terms of computation cost. A better solution seems to find other artificial boundary conditions which can be applied to a position not too far from the cylinder (or wire) and yield correct flow structure.

Another issue of the numerical work is about the boundary condition to be applied on the wire surface when the wire is heated by a constant power. If one neglects the wire thermal inertia the power used to heat the wire is transferred to the surrounding fluid, it means that on the wire surface $-\int_0^{2\pi} \lambda(\partial T/\partial r) r \, d\theta$ is a constant in time and it is a line source case. However, this does not imply that the heat flux on the wire surface is uniform (i.e. $-\lambda(\partial T/\partial r)$ on the wire surface is independent of θ) nor that the surface temperature of the wire is constant. As line-sources used in experiments are mainly thin wires heated by Joule effect, it is thought that the wires should be considered as isothermal and this will be discussed in detail.

In order to understand the physical problem and compare with the numerical results we also carried out an experimental investigation. A very thin bronze wire of 40 μm in diameter and 5.1 cm in length is immersed in liquid nitrogen. Temperature histories of the wire are measured and compared with numerical results. As the thermal inertia of a thin wire is very small, thin wires are the best line heat-sources one could find. They also make it possible to study heat transfer problems induced by a step heating because fluid will react instantaneously to the heating step due to the very small thermal inertia. In other words, thin wires heated by Joule effect produce nearly perfect heating steps at the solid–fluid interface, which is not the case when using a massive heater. Furthermore very small dimension of the wire and very small Biot numbers ($hR/\tilde{\lambda}$) suggest that temperature fields in wires can be supposed to be uniform and measured by wires' electrical resistance.

It is noted that a line-source combined with a heating step is commonly used for measuring thermal conductivity of fluids. This is the so-called transient hot-wire method [13–17]. In this case, one rather attempts to delay the onset of natural convection so that heat transfer between wire and fluid remains mainly conductive and experimental data fit better the theoretical prediction for conduction. Therefore wires are set vertically in experiments. Healy et al. [14] and Saito et al. [17] investigated numerically transient laminar natural convection induced by a vertical line heat source.

In next section experimental set-up will be presented, it will be followed by descriptions of governing equations and numerical methods. Results obtained will then be discussed before giving concluding remarks.

2. Experimental set-up

Experiments are performed in liquid nitrogen under atmospheric pressure and saturation conditions. A quasi-perfect thermostat is therefore achieved since any heat contribution to a saturated fluid is converted into latent heat. Only a slight temperature variation, less than 0.15 K, is observed between the free surface and the test cell due to hydrostatic overpressure. Furthermore the low temperature of this cryogenic fluid allows us to neglect radiation heat transfer. The line heat source is a phosphorus bronze wire of 40 μm in diameter and 5.1 cm long. The aspect ratio, equal to 1250, is thought to be high enough to reduce end effects. The tank is a cylindrical vessel of 15 cm in diameter and 50 cm in height. The immersion depth of the test cell is approximately 40 cm. Since bronze is thermoresistive, the wire is both a heater and a thermometer. Heat is supplied by Joule effect:

$$q_J(t) = \frac{U_w^2(t)}{\mathscr{R}_w(t)} \frac{1}{\pi DL} \tag{1}$$

The mean temperature of the wire is determined by measuring its electrical resistance. A prior calibration yields a linear relationship between electrical resistance and temperature in the considered temperature range:

$$\Delta T_w = T_w(t) - T_0 = \frac{\mathscr{R}_w(t) - \mathscr{R}_0}{\gamma R_0} \tag{2}$$

where $\gamma\mathscr{R}_0$ is constant and equal to 2.7×10^{-3} Ω/K.

The wire is connected to four supports (Fig. 1): the two internal contacts allow for voltage measurement while the two external pins are used as current supply. The voltage supports are copper made. They were designed with a large thermal inertia so that their temperature remains constant, equal to the bath temperature, thus providing well-known boundary conditions. Referring to Eq. (2), the variation of the electrical resistance as a function of time remains negligible since both wire superheat and bronze thermal coefficient are small. Then, in this particular case, generation of a heating step is achieved by means of a voltage step. The only noticeable difference is observed at the very beginning due to the significant temperature rise occurring at that stage. The highest shift in heating rate observed in experiments is below 3% of the step. A schematic diagram of the electric circuit is presented in Fig. 2. The wire of electrical resistance $\mathscr{R}_w(t)$ is connected in series with a resistor $\mathscr{R}_1$, a constant voltage unit $U_0(t)$ and a switching relay. The resistor $\mathscr{R}_1$ which is

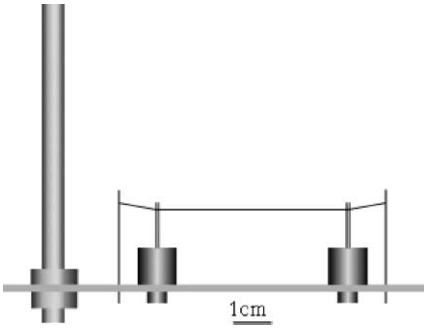

Fig. 1. Test cell.

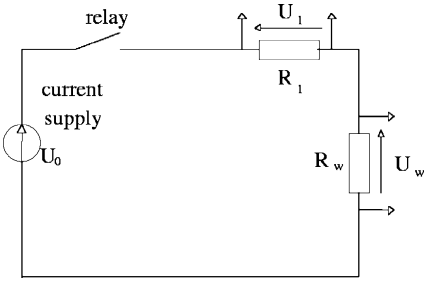

Fig. 2. Electrical circuit.

a 1 Ω/8 W type allows for current determination. Its value remains ultrastable ($\delta\mathscr{R}_1/\mathscr{R}_1 < 5 \times 10^{-4}$) regardless of the current intensity. The switch, a mercury relay is closed in less than 10 μs and it is therefore compliant with the expected time characteristics of the physical phenomena. Due to the very low temperature coefficient of the wire, two analog differential amplifiers with high impedance inputs are required in order to measure voltage changes at the wire and the resistor terminals, U_w and U_1 respectively. A detailed description of this specific device is available elsewhere [18]. The output amplified voltages are then connected to an eight-channel simultaneously sampling accessory which ensures a time skew between consecutive channels never larger than 50 ns. Data recording is finally performed using an acquisition board whose performance is 12-bit resolution (i.e. 2.44 mV in the voltage input range 0–10 V) and 250 kS/s. The sampling frequency used in experiments is 4000 Hz. The wire electrical resistance is calculated as follows:

$$\mathscr{R}_w(t) = \frac{U_w(t)\mathscr{R}_1}{U_1(t)} \tag{3}$$

Substituting $\mathscr{R}_w(t)$ in Eqs. (1) and (2), one obtains the average wire superheat and the heat flux supplied by Joule effect. Heat transfer to the fluid is written then:

$$q_f(t) = q_J(t) - (\widetilde{\rho}\widetilde{C})\frac{D}{4}\frac{dT_w}{dt} - \frac{Q_s(t)}{\pi DL} \tag{4}$$

where $Q_s(t)$ is the heating power lost by the wire supports. Even though this quantity remains delicate to predict accurately, it is easy to estimate its magnitude at steady-state. Since voltage supports are maintained at bath temperature, a classical fin model allows for the determination of temperature distribution within the wire. Heat lost by supports is thereafter derived using Fourier's law. Due to both wire dimensions and low overheatings involved in the process ($\Delta T < 30$ K), this quantity is always smaller than 5% of the total heat amount (see Appendix A and Table 1).

3. Mathematical equations and numerical methods

3.1. Governing equations

In this study fluid motion around the heating wire is assumed to be two-dimensional and liquid nitrogen is considered as a Newtonian fluid of density ρ, volumetric expansion coefficient β, thermal diffusivity κ (thermal conductivity λ and specific heat C_p) and kinematic viscosity ν. Boussinesq assumption is used although in the range of heating power considered temperature field may change some of the thermo-physical properties up to 50% (Fig. 3) [19]. For each heating power we use the values of thermal-physical properties at mean temperature, i.e., the average between measured wire temperature and ambient temperature, T_0. In polar coordinates the governing equations are then written:

Table 1
Wire overheating during later transients

Heat flux q (W/m^2)	ΔT_N (K)	ΔT_E (K)	Corrected ΔT_E (K)	Percentage of end effects (%)	Percentage of heat loss (%)
2.9×10^4	7.76	7.40 ± 0.02	7.75 ± 0.02	21	4.3
10^5	23.36	22.2 ± 0.4	23.2 ± 0.4	20	4

ΔT_N—Numerical results, ΔT_E—Experimental measurements, Corrected ΔT_E—Corrected experimental data by taking into account the end effects, Percentage of end effects—ratio between the length affected by end effects and total length of 5.1 cm and Percentage of heat loss—ratio between power lost through wire supports and the total heating power.

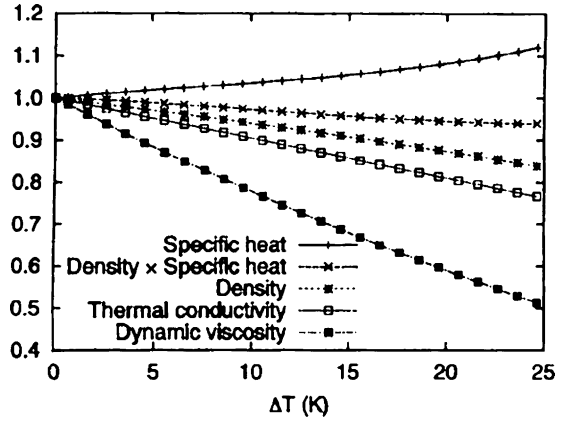

Fig. 3. Thermo-physical properties versus temperature overheating. At atmospheric pressure, the saturated temperature equal to 77.364 K is used as T_0 and the corresponding thermophysical properties [19] are $\rho = 807.4$ kg/m^3, $C_p = 2038$ J kg^{-1} K^{-1}, $\lambda = 0.01395$ W m^{-1}K^{-1} and $\mu = 1.64 \times 10^{-4}$ kg m^{-1} s^{-1}.

functions. Furthermore domain decomposition technique is associated with spatial discretisation in radial direction: $r \in [R, R']$ is divided into several sub-domains; in each sub-domain Chebyshev collocation method is used in radial direction and Fourier Galerkin method in the other one. Once applied to Eqs. (5) and (6) the resulted system consists of, apart from velocity–pressure coupling, Helmholtz equations. Due to the orthogonality of the Fourier modes, these Helmholtz equations reduce to K mono-dimensional linear equations which are solved by a direct LU factorisation (decomposition of a matrix into product of a lower and an upper triangular matrices). The coupling between diffusion operators for u and v can be classically alleviated by the change of variables $u^+ = u + \mathrm{i}v$ and $u^- = u - \mathrm{i}v$ [20]. The velocity–pressure coupling is handled by standard projection method making use of time-splitting [21]. At the sub-domain interfaces, we impose that the functions and their first normal derivatives on the interfaces are continuous. Further details on the numerical methods can be found in [22].

$$\begin{cases} \dfrac{\partial u}{\partial r} + \dfrac{u}{r} + \dfrac{1}{r}\dfrac{\partial v}{\partial \theta} = 0 \\ \dfrac{\partial u}{\partial t} + u\dfrac{\partial u}{\partial r} + \dfrac{v}{r}\dfrac{\partial u}{\partial \theta} - \dfrac{v^2}{r} = -\dfrac{1}{\rho}\dfrac{\partial p}{\partial r} + \nu\left[\left(\dfrac{\partial^2}{\partial r^2} + \dfrac{1}{r}\dfrac{\partial}{\partial r} - \dfrac{1}{r^2} + \dfrac{1}{r^2}\dfrac{\partial^2}{\partial \theta^2}\right)u - \dfrac{2}{r^2}\dfrac{\partial v}{\partial \theta}\right] - g\beta(T - T_0)\cos(\theta) \\ \dfrac{\partial v}{\partial t} + u\dfrac{\partial v}{\partial r} + \dfrac{v}{r}\dfrac{\partial v}{\partial \theta} + \dfrac{uv}{r} = -\dfrac{1}{\rho r}\dfrac{\partial p}{\partial \theta} + \nu\left[\left(\dfrac{\partial^2}{\partial r^2} + \dfrac{1}{r}\dfrac{\partial}{\partial r} - \dfrac{1}{r^2} + \dfrac{1}{r^2}\dfrac{\partial^2}{\partial \theta^2}\right)v + \dfrac{2}{r^2}\dfrac{\partial u}{\partial \theta}\right] + g\beta(T - T_0)\sin(\theta) \\ \dfrac{\partial T}{\partial t} + u\dfrac{\partial T}{\partial r} + \dfrac{v}{r}\dfrac{\partial T}{\partial \theta} = \kappa\left(\dfrac{\partial^2}{\partial r^2} + \dfrac{1}{r}\dfrac{\partial}{\partial r} + \dfrac{1}{r^2}\dfrac{\partial^2}{\partial \theta^2}\right)T \end{cases} \tag{5}$$

where t is the time, u and v are the radial and azimuthal velocity components, p is the pressure deviation from the hydrostatic pressure and T is the temperature.

If one desires to study the effects of wire thermal inertia during the transient, Eq. (5) should be coupled with the following heat conduction equation in the wire:

$$\widetilde{\rho}\widetilde{C}\frac{\partial T}{\partial t} = \widetilde{\lambda}\left(\frac{\partial^2}{\partial r^2} + \frac{1}{r}\frac{\partial}{\partial r} + \frac{1}{r^2}\frac{\partial^2}{\partial \theta^2}\right)T + Q_v \tag{6}$$

where Q_v is a uniform volumetric heat source.

3.2. Numerical methods

Eqs. (5) and (6) are discretised in time by a second-order scheme of finite difference type: for stability reasons the diffusion terms are treated implicitly while convective terms are treated explicitly. The periodicity in the azimuthal direction makes it natural to resort to spatial approximation based on tensor products of Chebyshev polynomials and Fourier series as basis

3.3. Boundary and initial conditions

As explained in Section 1, in external natural convection the physical domain is unbounded and main difficulties of numerical studies of such flows lie in the choice of artificial outer boundary of the computational domain and the corresponding flow conditions which are unknown. We first choose a radial position R' which is relatively large compared with R the wire radius in order to fix the computational domain $(r, \theta) \in [R, R'] \times [0, 2\pi]$. At $r = R'$, i.e. on the outer boundary, recently Kelkar and Choudhury [12] suggested a pressure condition under velocity–pressure (V–P) formulation. We used for velocity–pressure coupling the following conditions:

$$p = 0 \tag{7}$$

and

$$\left(\frac{\partial}{\partial r} + \frac{1}{r}\right)(u, v) = 0 \tag{8}$$

As for the temperature at $r = R'$ we used standard conditions: for inflow region temperature is set to the ambient value T_0 and for outflow region radial temperature gradient is set to zero [10], i.e.

$$\begin{array}{ll} T = T_0 & \text{if } u > 0 \\ \frac{\partial T}{\partial r} = 0 & \text{if } u < 0 \end{array} \tag{9}$$

As indicated in [10], this temperature condition in outflow region is not suitable for low Rayleigh number cases and further studies are required. Note, however, that in transient cases, the gradient condition is equivalent to $T = T_0$ before thermal plumes rise to the artificial outer boundary. The transient results presented in this paper are obtained before the plume front crosses the outer boundary.

On wire surface we apply no-slip conditions for velocity and constant heat transfer through wire surface:

$$u = v = 0 \tag{10}$$

and

$$-R\int_0^{2\pi} \lambda \frac{\partial T}{\partial r}\bigg|_R \mathrm{d}\theta = Q_L \tag{11}$$

where Q_L is the heating power or heat loss rate per unit length of the line source. As in the azimuthal direction flow field is periodic at constant r, it is natural to expand temperature into Fourier series: $T(r,\theta) = \sum_{k=0}^{\infty} \widehat{T}_k(r) \times \exp(\mathrm{i}k\theta)$. No matter which kind of boundary conditions for $\widehat{T}_k$ with $k \neq 0$, Eq. (11) reads always:

$$Q_L = -\sum_{k=0}^{\infty} R\lambda \frac{\partial \widehat{T}_k}{\partial r}\bigg|_R \int_0^{2\pi} \exp(\mathrm{i}k\theta)\,\mathrm{d}\theta = -2\pi R\lambda \frac{\partial \widehat{T}_{k=0}}{\partial r}\bigg|_R$$

which is a Neumann condition for $k = 0$. One can certainly impose for other k a homogeneous Neumann condition ($\partial \widehat{T}_k/\partial r = 0$) on the wire surface. This would mean that the temperature on the wire surface is non-uniform because $\partial \widehat{T}_k/\partial r = 0$ means $\widehat{T}_k \neq 0$. However it seems to us more reasonable to consider the wire as isothermal since the bronze wire used is a very good heat conductor compared with liquid nitrogen and the Biot number corresponding to the highest heating rate is smaller than 10^{-4}. One has therefore to find the uniform temperature which guarantees the global heat flux continuity. This can easily be realised in Fourier space: for the constant mode a constant heat flux is imposed while for the other modes we consider homogeneous Dirichlet condition, i.e. the coefficients of these Fourier modes are set to zero on the wire surface. The boundary conditions used for temperature on the wire surface are therefore the following combined Neumann–Dirichlet conditions:

$$\begin{array}{ll} -\lambda \frac{\partial \widehat{T}_k}{\partial r}\Big|_R = Q_L/(2\pi R) & \text{for } k = 0 \\ \widehat{T}_k(R) = 0 & \text{for } k \neq 0 \end{array} \tag{12}$$

For the coupled system consisting of Eqs. (5) and (6), Q_v is related to Q_L as following: $Q_L = \pi R^2 Q_v$. We applied heat flux conservation across the wire surface:

$$\lambda \frac{\partial T}{\partial r} = \widetilde{\lambda} \frac{\partial T}{\partial r} \tag{13}$$

Solving the coupled equations (5) and (6) makes it possible to not only check the validity of the proposed hybrid conditions—combined Neumann and Dirichlet conditions on the wire surface but also quantify the inertia of the bronze wire and its effects on the transients.

Initial conditions used in transient cases are $u = v = 0$ (liquid nitrogen motionless) and $T = T_0 = 77.364$ K which is the saturation temperature of liquid nitrogen at atmospheric pressure.

4. Results and discussions

In this section we first address the structure of 'steady' flows around a cylinder at a constant temperature in order to validate the methodology. Then we present numerical results and experimental measurements of transient natural convection flows and a comparison between numerical, experimental and analytical results: the validity of the proposed hybrid conditions on the wire surface is checked, the effects of the wire thermal inertia are quantified.

4.1. Benchmark solutions

The benchmark problem proposed by Saitoh et al. [11] concerns natural convection around a cylinder of constant surface temperature at Rayleigh numbers ranging from 10^3 to 10^5. Results in the literature have been mainly obtained with stream function–vorticity formulation and only one work [12] has been conducted with pressure–velocity formulation using a pressure boundary condition in the far-field.

It is first important to make clear that for external natural convection there is no steady state solution when the physical domain is unbounded. However it is possible to obtain steady solutions if one considers a limited region around the cylinder and the Rayleigh number is not very high.

Comparison between the present results and the benchmark solutions in the literature is performed for $Ra = 10^3$ and 10^4 and based on average Nusselt numbers (hD/λ) on cylinder surface. Nusselt numbers are calculated after steady conditions are achieved around the cylinder.

We used the pressure condition (Eq. (7)) associated with Eq. (8) for both Rayleigh numbers investigated: R' is fixed at $22.5R$ and a spatial resolution of 161×101 (8 sub-domains) is used. Concerning the corresponding steady states, Nusselt numbers are equal to 2.98 at

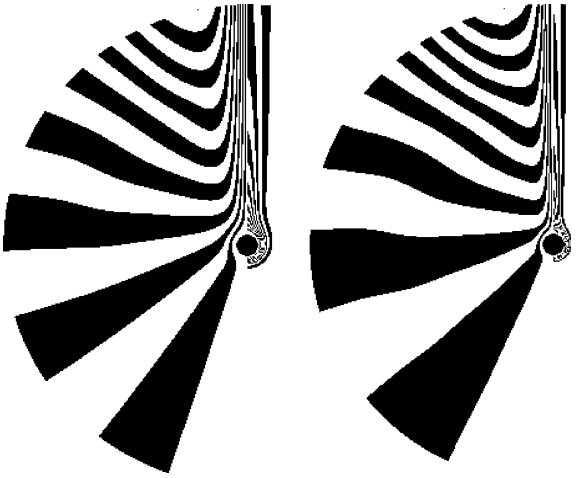

Fig. 4. Benchmark solutions at $Ra = 10^3$ (left) and $Ra = 10^4$ (right) obtained with pressure conditions—Eq. (8). Stream functions (left half) and temperature fields (right half) are presented in numerical interferogram form.

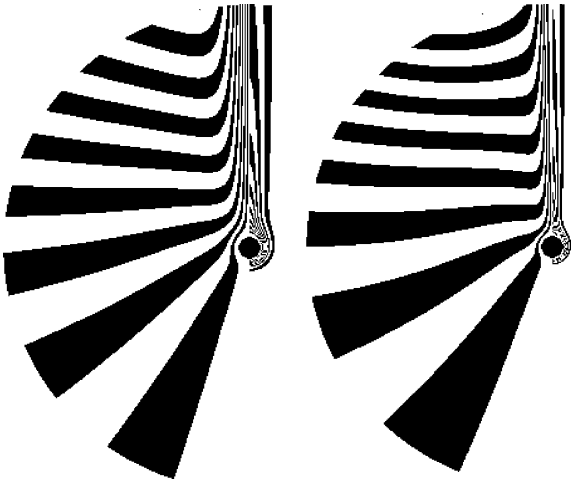

Fig. 5. Benchmark solutions at $Ra = 10^3$ (left) and $Ra = 10^4$ (right) obtained with conditions (14). Stream functions (left half) and temperature fields (right half) are presented in numerical interferogram form.

$Ra = 10^3$ and 4.77 at $Ra = 10^4$, which should be compared respectively with 3.024 and 4.826 provided by Saitoh et al. [11]. The difference is of order 1% and from this unique criterion the code can be considered as validated.

The corresponding flow structures are displayed in Fig. 4. They are similar to those reported in [12], but look quite different from those obtained by Saitoh et al. [11] when using a very large computational domain. The difference lies in that outside the thermal plume fluid motion is downward whereas Saitoh et al. showed an upward fluid motion. This downward fluid motion outside the thermal plume, which is also reported by other authors [10,12], is surprising and induced by the outer boundary conditions. In fact the pressure condition combined with homogeneous Neumann conditions for velocity implies that fluid flow is almost normal to the outer boundary.

In order to understand the influence of outer boundary conditions on flow structures, we implemented slightly different conditions:

$$\frac{p}{\rho} = v\left(\frac{\partial u}{\partial r} + \frac{u}{r}\right)$$
$$0 = v\left(\frac{\partial v}{\partial r} + \frac{v}{r}\right) \tag{14}$$

R' is set to $22.5R$ and a spatial resolution of 161×161 is used. Fig. 5 displays the corresponding flow structures. It can be seen that fluid motion outside the thermal plume is almost horizontal, which seems physically more reasonable. Note that although different outer boundary conditions yield different flow structures in the far field, near the cylinder velocity fields and temperature fields are very similar and Nusselt numbers are almost identical. It seems therefore that using Nusselt number as a unique criterion to characterise external natural convection is not sufficient. Since very few experimental results are available on velocity fields, no conclusion can be drawn so far on flow structures and further works are needed to determine far-field flow structure and identify the proper outer boundary conditions.

4.2. Transient problem

In the following we present the results obtained for two heat fluxes, $q = 2.9 \times 10^4$ and 10^5 W/m^2. Experimental data are compared with analytical solution of heat conduction and results obtained by using two types of numerical simulations: one neglects the wire thermal inertia and another takes it into account (conjugate heat transfer). Numerical simulations are performed with $R' = 500R$ and a spatial resolution of 161×141 (8 subdomains).

4.2.1. Transients without thermal inertia

Fig. 6 displays temperature histories of the wire obtained respectively from experiments and numerical simulation without thermal inertia. At first glance, even the experimental chart lies beneath numerical curve, both shapes look very similar: temperature first rises sharply, reaches a maximum, then decreases smoothly towards a constant value (which may be called steady state). Times corresponding to the maximum (temperature overshoot) are in good agreement as well as those for steady-state

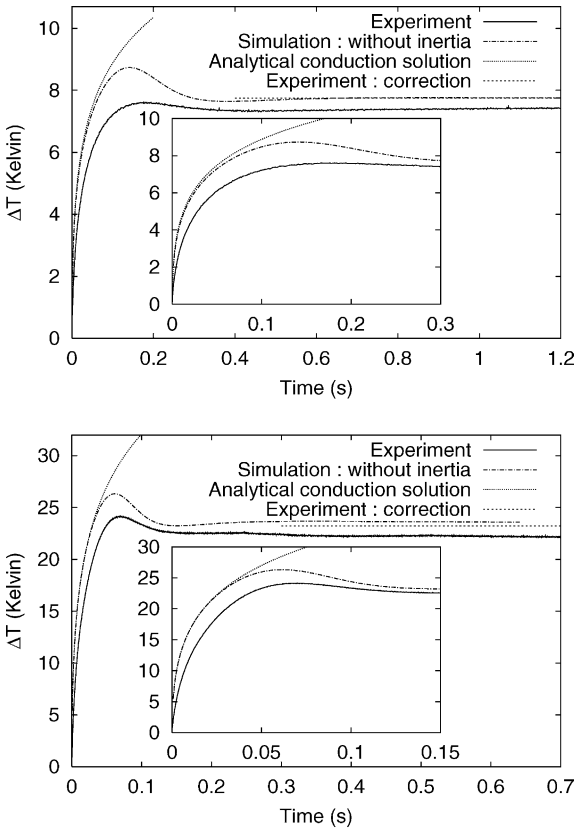

Fig. 6. Time evolutions of wire superheat: $q = 2.9 \times 10^4$ W/m^2 (top) and $q = 10^5$ W/m^2 (bottom).

achievement. The temperature difference observed at final stages can be noticeably reduced by considering end effects. Since both voltage supports are maintained at bath temperature, the wire superheat measured during experiments is inherently an average over the total wire length and its value is lower than the overheating in the central section. Simple theoretical analysis, detailed in Appendix A, attests that end effects occur on almost 20% of the total wire length. As numerical two-dimensional simulations are performed for an infinite line heat source, only uniform temperature in the central section has to be compared with numerical results (see Table 1 and Fig. 6). Plotting this value on the same figure, we observe better agreement between the results.

Concerning the earlier stages of the transients, heat transfer is achieved by pure conduction into the liquid. Neglecting in a first approximation the end effects, this configuration is equivalent to an infinite cylindrical heat source in a semi-infinite medium and isotherms are concentric cylinders. This transient, one-dimensional conduction problem has an analytical solution. Taking into account the wire diameter but neglecting its thermal inertia, heat transfer in the liquid may be predicted considering a hollow cylinder of outer radius R'. Temperature of liquid in contact with the wire surface reads (cf. Appendix B):

$$\Delta T(R,t) = \frac{Q_L}{\lambda}\left[\frac{1}{2\pi}\ln\left(\frac{R'}{R}\right) + \frac{1}{2R}\sum_{n=1}^{\infty} C_n(R)\exp(-\kappa\alpha_n^2 t)\right] \tag{15}$$

with coefficients

$$C_n(R) = J_0^2(R'\alpha_n)\frac{J_0(R\alpha_n)Y_1(R\alpha_n) - Y_0(R\alpha_n)J_1(R\alpha_n)}{\alpha_n[J_1^2(R\alpha_n) - J_0^2(R'\alpha_n)]}$$

The number of terms required to ensure convergence of the series at the r.h.s. of Eq. (15) is determined using the following criterion:

$$\Delta T(R,0) = 0$$

In the present calculation, a ratio R'/R equal to 100 is selected, 1500 terms yield $\Delta T(R,0) = 0.22$ K and 10 000 terms are required to obtain $\Delta T(R,0) = 0.034$ K.

As can be seen in the close-up (Fig. 6), there is a good agreement between theoretical solution of conduction and numerical simulation in the initial phase during which heat transfer is purely conductive. They indicate also the time at which convective effects become significant when both curves diverge. Concerning the difference between experimental and numerical solutions, it could result from the wire thermal inertia, the heat loss by wire's supports and the variation of liquid nitrogen's thermo-physical properties with temperature. In fact the total heat power supplied by Joule effect is not completely transferred to the fluid: part of it is used to heat the wire and part of it is lost through the supports. As the difference between experiments and numerical simulation is perceptible as soon as step begins, i.e. when wire superheats are very low and temperature rise is sharp, we therefore conclude that the wire thermal inertia must be taken into account.

4.2.2. Conjugate transients

In order to quantify inertia effects, another type of numerical simulations is performed by solving the coupled equations (5) and (6). Wire temperature is averaged over $(r,\theta) \in [0,R] \times [0,2\pi]$ so that it can be compared with experimental data. Temperature histories of the wire obtained for $q = 2.9 \times 10^4$ and 10^5 W/m^2 are plotted in Fig. 7 together with those obtained previously. During the early transient, temperature superheat in the conjugate case is different from that obtained without thermal inertia (the superheat is less important because wire retains part of the heating power) and it agrees better with experimental chart. In both cases temperature evolutions are the same at later time stages

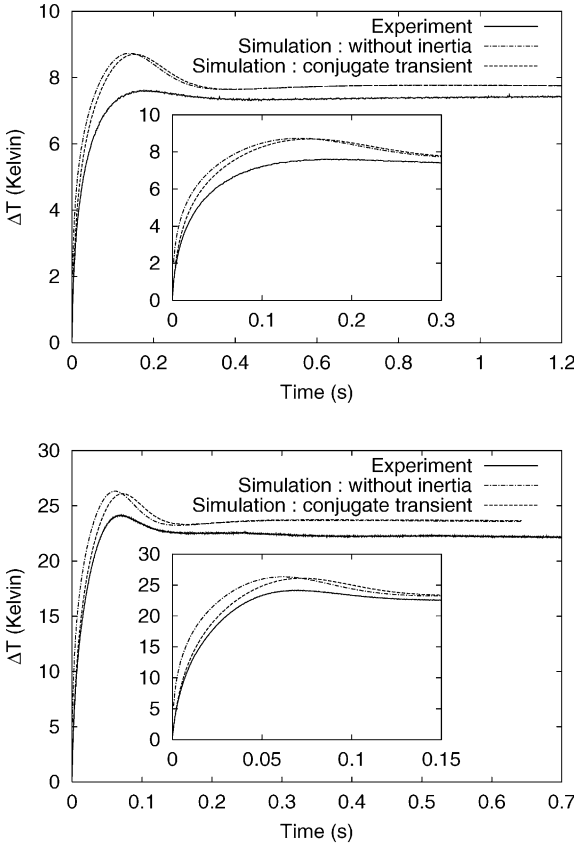

Fig. 7. Time evolutions of wire superheat during conjugate transients: $q = 2.9 \times 10^4$ W/m^2 (top) and $q = 10^5$ W/m^2 (bottom).

as it could be expected. This means that although the wire is extremely thin, its thermal inertia, no matter how small it is, cannot be neglected and plays an important role in early transients. One therefore has to take it into account as soon as an accurate prediction of early stages of the transients is requested, like for instance in transient hot wire method.

Note that despite the consideration of the thermal inertia there is still discrepancy between experimental data and numerical results during the later stages ($t > 0.01$ s). It seems that other effects come into play as time progresses. The discrepancy observed could result from three-dimensional end effects as well as from the variation of fluid properties with temperature. Further studies are thus necessary to minimise these effects or take them into account.

It is also to note that for both considered heat fluxes temperature distributions on the wire surface are visualised during numerical simulations: temperature is uniform there since the largest value of the non-constant temperature modes in Fourier space is about 2×10^{-6} of the superheat; the corresponding mode is $\exp(i\theta)$. We conclude that the hybrid temperature condition proposed for the wire surface stands.

4.2.3. Transient flow structures and scalings

Although inertia affects early stages of the transients, flow structures during the transients are very similar. Fig. 8 displays several instantaneous stream-functions and temperature fields during the transient produced by the heating step of 10^5 W/m^2, obtained without taking into account inertia effects.

Flow structures during the transient are similar to those presented by Saitoh et al. [11]. At the very beginning of the transient, heat transfer is conductive (isotherms are circles) and very weak flow is induced around the wire (flow is symmetrical about the vertical plane through the wire's axis and stream-functions are symmetrical about the horizontal plane through the wire's axis). Symmetry about the horizontal plane is broken later on (Fig. 8) due to the fact that hot fluid moves upwards: the centre of stream-function (the initial vortex) is located above the wire, isotherms below the wire are slightly squeezed and those above dilated.

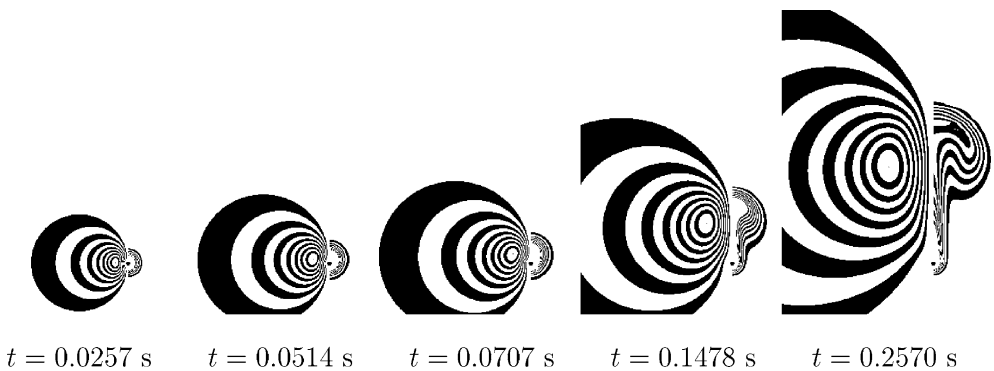

Fig. 8. Instantaneous stream-functions and temperature fields ($q = 10^5$ W/m^2).

Deformation of the isotherms is more pronounced when the superheat reaches its peak value ($t = 0.0707$ s). At this moment convection plays already an important role as the line heat source will be cooled down. With time advancing fluid motion continues to squeeze the isotherms, at $t = 0.1478$ s a 'mushroom' is formed due to the leading edge effect. The mushroom grows in time while the vortex centre moves up.

At $t = 0.3$ s the superheat of the line source reaches almost a constant value. Although there are no more changes in superheat, the mushroom and the initial vortex keep rising up and it is thus difficult to give a sense to steady state when the physical domain is unbounded. It only makes sense to conclude about steady state or steady solutions in a limited region around wires or cylinders.

Concerning the transients it is interesting to know how time and superheat scale with heating rate and therefore do some scale analyses. At the beginning of the transients, in the small region surrounding the wire thermal diffusion balances thermal inertia:

$$\frac{\Delta T}{t} \sim \kappa \frac{\Delta T}{\delta r^2}$$

where δr characterises the extension of non-isothermal zone. One gets $t \sim \delta r^2/\kappa$. Within δr there will be balance either between buoyancy and inertia or between buoyancy and friction:

$$\frac{v}{t} \sim \kappa \frac{v}{\delta r^2} \sim g\beta\Delta T \quad \text{or} \quad v\frac{v}{\delta r^2} \sim g\beta\Delta T$$

One can see that inertia differs from friction only by a factor of Pr and for Pr of $\mathcal{O}(1)$ they are of the same order. These relations stand until convective term in energy equation reaches thermal diffusion or inertia:

$$v\frac{\Delta T}{\delta r} \sim \kappa \frac{\Delta T}{\delta r^2}$$

Considering the fact that on the wire surface $q \sim \lambda\Delta T/\delta r$, one obtains the following relations for the convection onset:

$$\delta r \sim \left(\frac{\lambda v\kappa}{g\beta q}\right)^{1/4} \quad t \sim \sqrt{\frac{\lambda v}{\kappa g\beta q}} \quad v \sim \kappa\left(\frac{g\beta q}{\lambda v\kappa}\right)^{1/4}$$

$$\Delta T \sim \frac{q}{\lambda}\left(\frac{\lambda v\kappa}{g\beta q}\right)^{1/4}$$

Therefore concerning the convection onset, time scales as $q^{-1/2}$, superheat ΔT behaves as $q^{3/4}$ and velocity scales as $q^{1/4}$. Analyses beyond this time scale are more complicated. It is noted that before set-up of convective motion the process is purely conductive: superheat ΔT is linear with q and that δr and t are independent of q (it means that at a given time t the extension of the non-isothermal zone is independent of heat flux q). The scaling we proposed will not stand for the very initial phase of transients. One may hope on the other hand that $q^{3/4}$ and q give the lower and upper bounds to the scaling of superheat ΔT on the wire surface.

In order to check the scaling analyses we performed simulations of four transients by using the thermophysical properties of liquid nitrogen at $T = 80$ K and neglecting the wire thermal inertia. The corresponding results, evolutions in time of temperature above the wire along the symmetry line of thermal plume, are plotted with different scales in Fig. 9. On the wire surface temperature scales as q in the very initial phase and its long time behaviour is limited by $q^{3/4}$ and q, which agrees well with the scaling analyses. For other points monitored $q^{3/4}$ is the upper bound of temperature scaling, i.e. $\Delta T \sim q^a$ with $a < 3/4$. As for the convection set-up and transients, time scales as $q^{-1/2}$: with this scaling temperature peaks occur at the same time and time evolutions collapse almost on one curve. Despite the fact that the scale of $t \sim q^{-1/2}$ is obtained for convection set-up, it seems to characterise well long time behaviour of the transients. Note nevertheless that well above the wire (at $29R$, $45R$ and $61R$ for example) time scales of both the plume front and the temperature peaks behave slightly different from $q^{-1/2}$.

In dimensionless form this will mean that time scale is in inverse proportion to the square root of Rayleigh number based on heat flux and wire radius. This square root relationship is well known for internal natural convection at high Rayleigh numbers. What is surprising is that it holds for the heating rates and wire diameter considered here which correspond to very small Rayleigh numbers (<1).

5. Summary and concluding remarks

We have performed both experimental and numerical studies on the onset of natural convection induced by a step heating around a line heat source. The heating element used is a thin bronze wire of 40 μm in diameter and 5.1 cm long. The working fluid is liquid nitrogen. Results were mainly obtained for two heat fluxes of 2.9×10^4 and 10^5 W/m^2.

In terms of the time scale of the convective motion onset and the final wire superheat there is a good agreement between the numerical and experimental results. Transients can be described as follows: at the beginning, due to the poor efficiency of conductive heat transfer, a sharp increase of the wire temperature is observed and a maximum is rapidly achieved. At this particular moment, isotherms in the fluid display an ovoid form and convection effects become significant. The leading edge effect then squeezes the top part of the isotherms and results in

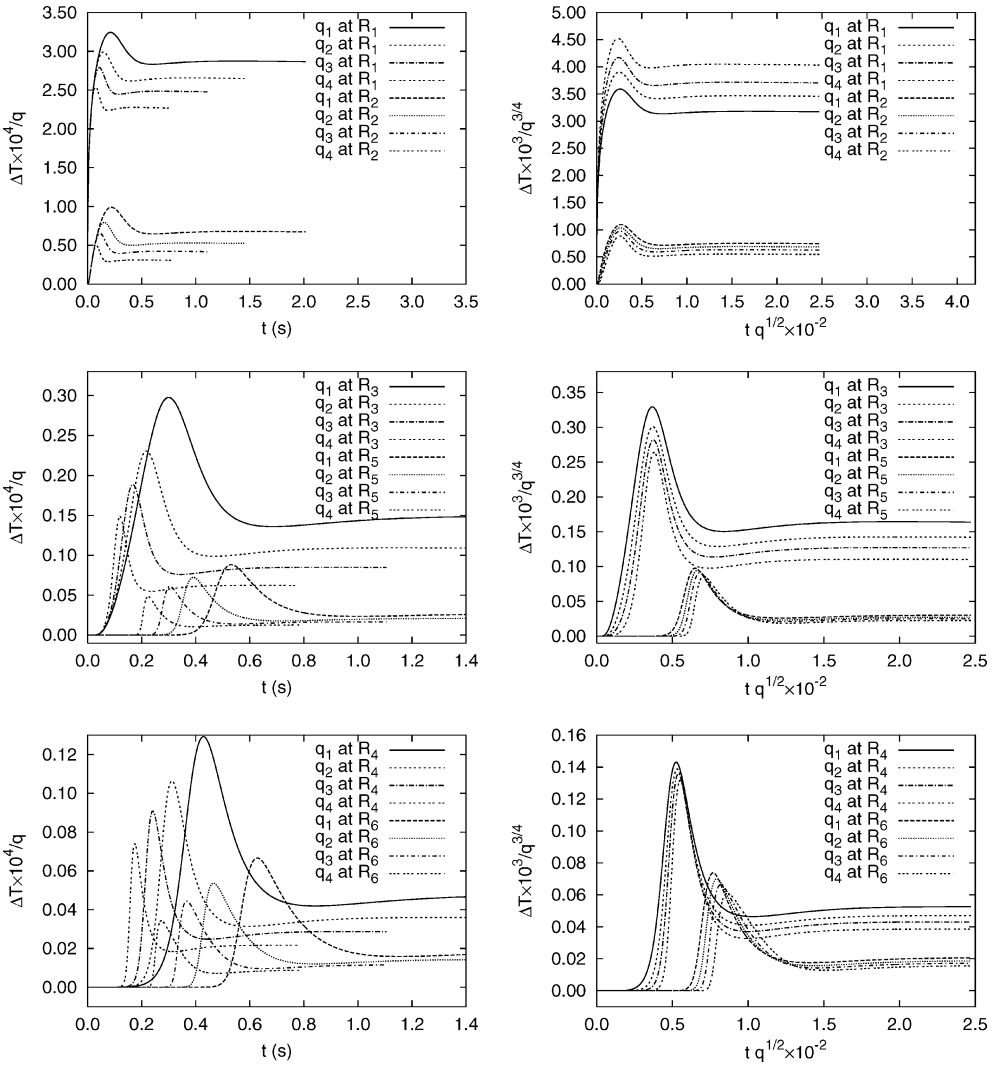

Fig. 9. Scalings of temperature field along symmetry line of thermal plumes during transients ($q_1 = 1.5 \times 10^4$ W/m^2, $q_2 = 2.9 \times 10^4$ W/m^2, $q_3 = 5 \times 10^4$ W/m^2, $q_4 = 10^5$ W/m^2; $R_1 = R$, $R_2 = 5R$, $R_3 = 13R$, $R_4 = 29R$, $R_5 = 45R$, $R_6 = 61R$). On the wire surface $\Delta T \sim q$ during initial phase and is limited by $q^{3/4}$ and q in convective regime. Time scale of convective motion behaves like $q^{-1/2}$ and well above the wire $q^{3/4}$ provides the upper bound of ΔT.

a slight decrease of the wire temperature and the formation of a 'mushroom' (head of a thermal plume). The 'mushroom' keeps progressing upwards and has little influence on the wire temperature that tends to an asymptotic value. Isotherms near the wire are in forms of cone and steady conditions are observed.

Scaling analyses were carried out and provide, for the transients of natural convection around thin wires, the following results which are confirmed by numerical simulations: On the wire surface $\Delta T \sim q$ during initial phase and is limited by $q^{3/4}$ and q after convection set-up. Time scale of convective motion behaves like $q^{-1/2}$ and well above the wire $q^{3/4}$ provides the upper bound of ΔT.

Further comparison between numerical and experimental results discloses the following points:

- Thermal inertia of a line heat source is significant at early stages and has therefore to be considered if an accurate prediction is desired. For example it seems mandatory to take wire's thermal inertia into account for applications of transient hot-wire method.
- Even for the high aspect ratio considered in the present experiment ($L/D > 1000$), three-dimensional end effects take place on almost 20% of the wire length and are likely to be the main reason of the discrepancy observed between numerical simulations and experiments.

Numerical simulations performed in the present work, using a velocity–pressure formulation, show that:

- A hybrid condition, combining Dirichlet and Neumann conditions, is appropriate on the wire surface since it takes into account the prescribed heating rate as well as the uniform temperature of a line heat source. A uniform heat flux condition is not suitable in this particular thin wire case.
- The flow conditions used, i.e. Eq. (8), at the artificial outer boundary of the computational domain, yield similar results as the pressure condition suggested by Kelkar and Choudhury [12], but the flow structure is different from that obtained by using a very large computational domain [11]. It is concluded that the stress-free conditions used in the present work and those used by Kelkar and Choudhury [12] are not the appropriate conditions in the sense that, assuming the computation in the large domain is correct, they fail to reproduce the corresponding flow structure.

Although the benchmark solutions provided by Saitoh et al. [11] are physically more plausible, the lack of experimental data makes difficult to conclude on the real flow structure around thermal plumes. Even though the problem is not new and accurate temperature fields delivered by holographic interferometry are available in the literature, more experiments, especially those measuring velocity fields, are needed to shed light on the flow structure of thermal plumes and provide reference for numerical simulations. Such measurements can be obtained by particle image velocimetry (PIV) for instance. Let us stress that numerical studies of external natural convection are quite few compared with those of internal natural convection (rectangular and circular enclosures for example). This is probably due to the fact that far flow fields and consequently the numerical conditions to be applied are not well known. More investigations of external natural convection should be encouraged to work out the far field flow conditions, which is the main difficulty to be overcome when doing numerical studies of such flows.

Acknowledgements

The computations have been performed at the Centre Informatique National de l'Enseignement Supérieur (CINES).

Appendix A. Temperature distribution in the wire at steady-state

We consider a thin wire along which an electric current of constant strength I is flowing. Both ends are at prescribed temperature T_0 and temperature profile is symmetrical about the middle of the wire. The wire (radius R and length L) is in a surrounding medium at temperature T_0 in which heat is released with a heat transfer coefficient h. Considering steady-state conditions, the problem reads [23, p. 152]:

$$\frac{\mathrm{d}^2T}{\mathrm{d}x^2}-\frac{2h}{\lambda R}(T-T_0)=-\frac{\omega}{\lambda}$$

where ω is the internal heat generation (W/m^3) defined as $\mathscr{R}I^2/\pi R^2L$.

If the electrical resistivity of the wire varies linearly with temperature, one obtains $\mathscr{R}=\mathscr{R}_0[1+\gamma(T-T_0)]$.

Equation of heat conduction reads:

$$\frac{\mathrm{d}^2(T-T_0)}{\mathrm{d}x^2}-\alpha^2(T-T_0)=-\frac{\omega_0}{\lambda}$$

where

$$\alpha^2=\frac{2h}{\lambda R}-\frac{\mathscr{R}_0\gamma I^2}{\lambda\pi R^2L}\quad\text{and}\quad\omega_0=\frac{\mathscr{R}_0I^2}{\pi R^2L}$$

In the case of α^2 positive, temperature distribution along the wire is given by

$$T(x)=T_0+\frac{\omega_0}{\lambda\alpha^2}\left(1-\frac{\cosh(\alpha x)}{\cosh(\alpha L/2)}\right)\tag{A.1}$$

Heat loss rate by supports can be derived from Fourier's law:

$$Q_\mathrm{s}=-2\pi R^2\lambda\left.\frac{\mathrm{d}T}{\mathrm{d}x}\right|_{x=L/2}=2\pi R^2\omega_0\tanh(\alpha L/2)/\alpha$$

and the relative heat loss is then $Q_\mathrm{s}/(\mathscr{R}I^2)$.

The superheat is obtained then by averaging $T(x)-T_0$ over the wire length L:

$$\Delta T=\frac{\omega_0}{\lambda\alpha^2}\left(1-\frac{\tan\mathrm{h}(\alpha L/2)}{\alpha L/2}\right)\tag{A.2}$$

For experimental results reported in the present paper, the following parameters are available at any time: heat flux supplied by Joule effect q_J, current intensity in the wire I and the wire overheating averaged along the wire length ΔT. After ΔT reaches its asymptotic value, these parameters become constant and the theoretical results presented above can be used to determine the temperature distribution in the wire.

Given a constant value of ΔT, α is obtained by solving Eq. (A.2) and then used to calculate, according to Eq. (A.1), the temperature profile in the wire which is plotted below for both heat fluxes $q=2.9\times10^4$ and 10^5 W/m^2:

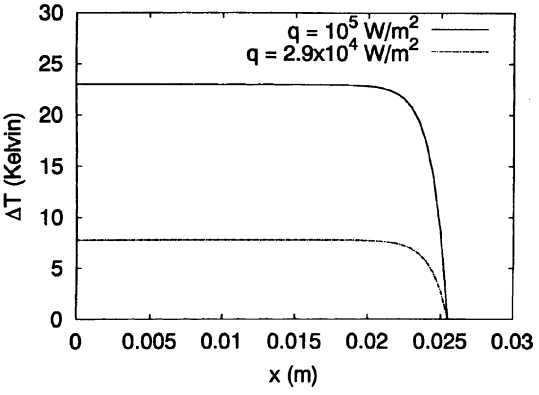

Appendix B. 1D transient heat conduction in a hollow cylinder

A motionless medium of thermal conductivity λ and thermal diffusivity κ bounded by two circular surfaces of respective radii R and R' ($R' > R$), is considered. Initial and boundary conditions are as follows: $T(r,0) = T_0$ at $t = 0$ for $r \geqslant R$, $Q_L = -2\pi R\lambda(\partial T/\partial r)$ at $r = R$ for $t > 0$ and $\lim_{r\to\infty} T(r,t) = T_0$ for $t > 0$.

The heat diffusion equation to be solved is

$$\frac{\partial T}{\partial t} = \kappa\left(\frac{\partial^2 T}{\partial r^2} + \frac{1}{r}\frac{\partial T}{\partial r}\right)$$

The solution is written [23, p. 203]:

$$\Delta T(r,t) = \frac{Q_L}{\lambda}\left[\frac{1}{2\pi}\ln\left(\frac{R'}{r}\right) + \frac{1}{2R}\sum_{n=1}^{\infty} C_n(r)\exp(-\kappa\alpha_n^2 t)\right]$$

where coefficients

$$C_n(r) = J_0^2(R'\alpha_n) \times \frac{J_0(r\alpha_n)Y_1(R\alpha_n) - Y_0(r\alpha_n)J_1(R\alpha_n)}{\alpha_n[J_1^2(R\alpha_n) - J_0^2(R'\alpha_n)]} \quad \text{and} \quad \alpha_n$$

are the positive roots of the following transcendental equation:

$$J_1(R\alpha)Y_0(R'\alpha) - Y_1(R\alpha)J_0(R'\alpha) = 0$$

J_0 and J_1 are Bessel functions of the first kind of order zero and one while Y_0 and Y_1 are Bessel functions of the second kind of order zero and one.

References

[1] K. Kitamura et al., Heat transfer and fluid flow of natural convection around large horizontal cylinders, Int. J. Heat Mass Transfer 42 (1999) 4093–4106.

[2] A. Linan, V. Kurdyomov, Laminar free convection induced by a line heat source and heat transfer from wires at small Grashof numbers, J. Fluid Mech. 362 (1998) 199–227.

[3] G.A. Ostroumov, Unsteady heat convection near a horizontal cylinder, Sov. Phys. Tech. Phys. 1 (12) (1956) 2627–2641.

[4] A.W. Schorr, B. Gebhart, An experimental investigation of natural convection wakes above a line heat source, Int. J. Heat Mass Transfer 13 (1970) 557–571.

[5] H. Yosinobu, Y. Onishi, S. Amano, S. Enyo, S. Wakitani, Experimental study on instability of a natural convection flow above a horizontal line heat source, J. Phys. Soc. Jpn. 47 (1) (1979) 312–319.

[6] B. Gebhart, L. Pera, A.W. Schorr, Steady laminar natural convection plumes above a horizontal line heat source, Int. J. Heat Mass Transfer 13 (1970) 161–171.

[7] C.A. Hieber, E.J. Nash, Natural convection above a line source: higher-order effects and stability, Int. J. Heat Mass Transfer 18 (1975) 1473–1478.

[8] T. Fujii, I. Morioka, H. Uehara, Buoyant plume above a horizontal line heat source, Int. J. Heat Mass Transfer 16 (1973) 755–768.

[9] B. Farouk, S.I. Güçeri, Natural convection from a horizontal cylinder—laminar regime, J. Heat Transfer 103 (1981) 522–527.

[10] P. Wang, R. Kahawita, T.H. Nguyen, Numerical computation of the natural convection flow about a horizontal cylinder using splines, Num. Heat Transfer A 17 (1990) 191–215.

[11] T. Saitoh, T. Sajiki, K. Maruhara, Bench mark solutions to natural convection heat transfer problem around a horizontal cylinder, Int. J. Heat Mass Transfer 36 (1993) 1251–1259.

[12] K.M. Kelkar, D. Choudhury, Numerical method for the prediction of incompressible flow and heat transfer in domains with specified pressure boundary conditions, Num. Heat Transfer B 38 (2000) 15–36.

[13] C.A. Nieto de Castro, J. Calado, W. Wakeham, M. Dix, An apparatus to measure the thermal conductivity of liquids, J. Phys. E 9 (1976) 1073–1080.

[14] J.J. Healy, J.J. de Groot, J. Kestin, The theory of the transient hot-wire method for measuring thermal conductivity, Physica C (1976) 392–408.

[15] X.G. Liang, The boundary induced error on the measurement of thermal conductivity by transient hot-wire method, Meas. Sci. Technol. 6 (1995) 467–471.

[16] M.J. Assael, L. Karagiannidis, N. Malamataris, W. Wakeham, The transient hot-wire technique: a numerical approach, Int. J. Thermophys. 19 (2) (1998) 379–389.

[17] A. Saito, K. Matsumoto, Y. Utaka, Reconsideration of the transient line heat source technique (analytical discussion on the influence of natural convection), JSME Int. J. 30 (270) (1987) 1935–1942.

[18] M.-C. Duluc, G. Defresne, M.X. François, Transient boiling on thin wires in liquid nitrogen, Adv. Cryog. Eng. B 45 (2000) 1237–1243.

[19] Selected Cryogenic Data Notebook, Bubble Chamber Group, Brookhaven National Lab., 1968.

[20] T.A. Patera, S.A. Orzag, in: Nonlinear Problems: Present and Future, North Holland, Armsterdam, 1982, p. 367.

[21] J.-L. Guermond, L. Quartapelle, On stability and convergence of projection methods based on pressure Poisson

equation, Int. J. Num. Meth. Fluids 26 (9) (1998) 1039–1053.

[22] O. Louchard, A. Randriamampianina, E. Leonardi, Spectral domain decomposition technique for the incompressible Navier–Stokes equations, Num. Heat Transfer A 34 (5) (1999) 495–518.

[23] H.S. Carslaw, C. Jaeger, Conduction of Heat in Solids, second ed., Clarendon Press, Oxford, 1959.